

# Optimization of the Qubit Coupled Cluster Ansatz on classical computers

Ilya G. Ryabinkin,<sup>1,\*</sup> Seyyed Mehdi Hosseini Jenab,<sup>1</sup> and Scott N. Genin<sup>1</sup>

<sup>1</sup>OTI Lumionics Inc., 3415 American Drive Unit 1, Mississauga, Ontario L4V 1T4, Canada

Immense interest in quantum computing has prompted development of electronic structure methods that are suitable for quantum hardware. However, the slow pace at which quantum hardware progresses, forces researchers to implement their ideas on classical computers despite the obvious loss of any “quantum advantage.” As a result, the so-called *quantum inspired* methods emerge. They allow one to look at the electronic structure problem from a different angle; yet, to fully exploit their capacity, efficient implementations are highly desirable. Here we report two schemes for improving the amplitude optimisation in the iterative qubit coupled cluster (iQCC) method—a variational quantum eigensolver-type approach which is based on the qubit coupled cluster (QCC) Ansatz. Our first scheme approximates the QCC unitary as a sum of symmetrical polynomials of generators up to a given order. The resulting energy expression allows for a flexible control of computational complexity via the order parameter. It also guarantees smoothness of trial energies and their derivatives, which is important for gradient-based optimization strategies. The second scheme limits the size of the expansion space in which the QCC unitary is generated. It provides better control of memory requirements, but in general may lead to the non-smooth variation of energy estimates upon changes in amplitudes. It can be used, however, to extrapolate energies for a given set of amplitudes towards the exact QCC value. Both schemes allow for a larger number of generators to be included into the QCC form compared to the exact formulation. This reduces the number of iterations in the iQCC method and/or leads to higher accuracy. We assess capabilities of the new schemes to perform QCC amplitudes optimization for a few molecular systems: dinitrogen ( $N_2$ , 16 qubits), water ( $H_2O$ , 36 qubits), and tris(2-(2,4-difluorophenyl)pyridine) iridium(III), ( $Ir(F_2ppy)_3$ , 80 qubits).

## I. INTRODUCTION

Quantum computing is a rapidly evolving area of computational science that employs engineered quantum systems—quantum computers—to perform calculations that are otherwise difficult for classical computers [1–3]. One of the promising applications of quantum computing is finding the electronic structure [4] of molecules and materials to model their chemical and optical properties [5]. Solving the electronic structure problem amounts to finding eigenvalues—ground and excited states—of the electronic Hamiltonian of a system of interest. The first method proposed for solving this problem on quantum computers was the quantum phase estimation (QPE) algorithm [6–12]. It quickly became clear, however, that reliable estimate of eigenvalues with QPE requires very complex quantum circuits and long coherence times. For example, simulations of the electronic structure of the iron-molybdenum cofactor (FeMoco)—an active site of Mo-dependent nitrogenase—were estimated to use an astronomical ( $10^{14} – 10^{16}$ ) number of T-gate operations with run time varying from a few months to several years [13]. Subsequently, the variational quantum eigensolver (VQE) [14–19] was suggested as a more frugal alternative to QPE. The VQE method finds the ground electronic state of an arbitrary qubit Hamiltonian

$$\hat{H} = \sum_i C_i \hat{P}_i, \quad (1)$$

in which  $C_i$  are numerical coefficients and

$$\hat{P}_i = \hat{\sigma}_{i_1} \dots \hat{\sigma}_{i_q}, \quad 0 \leq q \leq (n - 1) \quad (2)$$

are tensor products of Pauli elementary qubit operators  $\hat{\sigma}_j \in \{\hat{x}_j, \hat{y}_j, \hat{z}_j\}$  for  $n$  qubits (“Pauli words” for short). In the context of the electric structure problem, the Hamiltonian (1) is derived from the active-space electronic Hamiltonian of a molecular system [4] using fermion-to-qubit mappings, such as Jordan–Wigner (JW), Bravyi–Kitaev (BK) or the more recent ternary-tree mapping [20, 21]. Trial energy

$$E(\mathbf{t}) = \langle 0 | \hat{U}^\dagger(\mathbf{t}) \hat{H} \hat{U}(\mathbf{t}) | 0 \rangle \quad (3)$$

is evaluated on a quantum computer by measuring  $\hat{P}_i$  in Eq. (1) on a state  $\hat{U}(\mathbf{t})|0\rangle$  of a quantum register [22–27] and summing up the outcomes with coefficients  $C_i$ . Here,  $\hat{U}(\mathbf{t})$  is a parametrized unitary which must be realized as a quantum circuit and  $|0\rangle$  is a reference (initial) qubit state. Subsequently, the measured trial energies  $E(\mathbf{t})$  for different values of parameters  $\mathbf{t} = t_1, t_2, \dots$  are passed to a *classical* computer to find a minimum with respect to  $\mathbf{t}$ . By the variational principle,

$$\min_{\mathbf{t}} E(\mathbf{t}) \geq E_0, \quad (4)$$

where  $E_0$  is the exact ground-state energy of the Hamiltonian  $\hat{H}$ . We note that not only energies, but also energy gradients can be measured using a parameter-shift rule [28–30], which allows for using more efficient gradient-based minimization techniques.

The parametrized unitary  $\hat{U}(\mathbf{t})$  is a central quantity in VQE [14–19, 31–36]. Different flavours of VQE differ in

\* ilya.ryabinkin@otilumionics.com

the way how  $\hat{U}(\mathbf{t})$  is constructed. One specific form is the qubit coupled cluster (QCC) Ansatz [32] inspired by the variational approach introduced in Ref. 31. It is defined as a product of exponents of generators  $\hat{T}_k$ ,

$$\hat{U}(\mathbf{t}) = \prod_{k=1}^M \exp\left(-it_k \hat{T}_k/2\right), \quad (5)$$

that are themselves Pauli words. Initially, it was proposed to screen the entire space of all possible  $\hat{T}_k$  whose dimensionality is  $4^n$ , to include only generators that have non-zero values of the first energy derivatives

$$g_k = \frac{dE[\hat{T}_k]}{dt} = -\frac{i}{2} \langle 0 | [\hat{H}, \hat{T}_k] | 0 \rangle, \quad (6)$$

where  $[\hat{H}, \hat{T}_k]$  is a commutator. It was later recognized [37] that exponentially hard screening can be replaced by a *construction* of all such generators given the qubit Hamiltonian, and this procedure has linear complexity with respect to the number of terms in  $\hat{H}$ . If  $\hat{H}$  is a qubit image of the molecular electronic Hamiltonian, the proposed algorithm produces qubit analogs of all single and double excitations for a given set of molecular orbitals. The corresponding Ansatz is, therefore, similar to the factorized (“disentangled”) [38–40] form of a generalized unitary coupled cluster (GUCC) wave function [17, 41, 42]. Reference 37 also introduces an iterative scheme of building the QCC form *and* transforming Hamiltonian, which allows for systematic convergence of energy estimates to the exact ground-state energy of a given  $\hat{H}$ . If all steps, including evaluation and optimization of trial electronic energies (3), are done by a classical computer, this iterative qubit coupled cluster (iQCC) method becomes a quantum inspired algorithm.

The iQCC method [37] can use as few as one generator per iteration at expense of more iterations. Every iteration produces a new dressed Hamiltonian

$$\hat{H}^{(i)} = \left( \hat{U}^{(i)}(\mathbf{t}_{\text{opt}}^{(i)}) \right)^\dagger \hat{H}^{(i-1)} \hat{U}^{(i)}(\mathbf{t}_{\text{opt}}^{(i)}), \quad i = 1, \dots \quad (7)$$

where  $\hat{H}^{(i)}$  is the Hamiltonian at the  $i$ -th iteration,  $\hat{H}^{(0)}$  is the initial qubit-mapped active-space electronic Hamiltonian, and  $\hat{U}^{(i)}(\mathbf{t}_{\text{opt}}^{(i)})$  is a QCC unitary constructed at the  $i$ -th iteration evaluated at the optimized values of amplitudes  $\mathbf{t}_{\text{opt}}^{(i)}$ . However, dressing causes the Hamiltonian to quickly expand [43], taxing CPU and memory of a classical

computer. Additionally, using only a small number of generators poses a dilemma of artificial symmetry breaking, if not all generators that preserve local or approximate symmetries can be included into the Ansatz. Thus, enabling lengthier QCC Ansätze improves computational efficiency of the iQCC method making it competitive to the “traditional” quantum chemistry methods.

The current paper reports algorithm developments that allow as many as hundred thousands of generators to be simultaneously optimized. We propose two different approaches to simplify evaluation and optimization of trial energies given by Eq. (3). In the first one, we expand the QCC unitary (5) in a series where terms are symmetric polynomials of generators and retain all low-order terms up to a certain order. In the second, we recursively construct a trial qubit state  $\hat{U}(\mathbf{t})|0\rangle$  and drop the terms with smallest numerical coefficients to keep the total number of them fixed.

We use three molecular systems in our study: dinitrogen ( $N_2$ , 16 qubits), water ( $H_2O$ , 36 qubits), and Tris[2-(2,4-difluorophenyl)pyridine]Ir(III) ( $(Ir(F_2ppy)_3$ , 80 qubits) [44–46]. For the first system we consider molecular configurations with equilibrium N–N distance (a weakly correlated case) and a highly stretched geometry (a strongly correlated case), as well as compute the entire potential energy curve (PEC) to study the convergence of energy and amplitudes in transition from one to another. Water molecule is an illustration of an extrapolation technique using the second scheme. Finally, the last system is used to demonstrate scalability of our approach to large, industrially relevant molecules.

## II. THEORY

### A. Symmetric-polynomial expansion of the QCC unitary

Every exponent in the QCC Ansatz (5) can be evaluated in a closed form as

$$\exp(-it\hat{T}/2) = \cos(t/2) - i \sin(t/2) \hat{T}, \quad (8)$$

because any Pauli word is *involutory*,  $\hat{T}^2 = \hat{\mathcal{E}}$ , where  $\hat{\mathcal{E}}$  is the identity operator. There are  $2^M$  algebraic-independent terms in a superposition which encodes the state  $\hat{U}(\mathbf{t})|0\rangle$  on a quantum computer. This exponential complexity is a clear obstacle for classical computers.

Expanding the product in the right-hand side of Eq. (5) using the identity (8) we obtain

$$\begin{aligned}
\hat{U}(\mathbf{t}) &= \prod_{k=1}^M \cos(t_k/2) - i \sum_{j=1}^M \sin(t_j/2) \hat{T}_j \prod_{k \neq j}^M \cos(t_k/2) \\
&\quad - \sum_{i < j}^M \sin(t_i/2) \sin(t_j/2) \hat{T}_i \hat{T}_j \prod_{k \neq \{i,j\}}^M \cos(t_k/2) + \dots \\
&= \prod_{k=1}^M \cos(t_k/2) \left( 1 - i \sum_{j=1}^M \tan(t_j/2) \hat{T}_j - \sum_{i < j}^M \tan(t_i/2) \tan(t_j/2) \hat{T}_i \hat{T}_j + \dots \right)
\end{aligned} \tag{9}$$


---

Equation (9) uses specific grouping of terms that can be

better explained on the following simple example. Consider a unitary (5) with  $M = 3$  generators:

$$\begin{aligned}
\hat{U}(t_1, t_2, t_3) &= c_1 c_2 c_3 \quad (0\text{-th order}) \\
&\quad - i \left( s_1 c_2 c_3 \hat{T}_1 + c_1 s_2 c_3 \hat{T}_2 + c_1 c_2 s_3 \hat{T}_3 \right) \quad (1\text{-st order}) \\
&\quad - \left( s_1 s_2 c_3 \hat{T}_1 \hat{T}_2 + s_1 c_2 s_3 \hat{T}_1 \hat{T}_3 + c_1 s_2 s_3 \hat{T}_2 \hat{T}_3 \right) \quad (2\text{-nd order}) \\
&\quad + i s_1 s_2 s_3 \hat{T}_1 \hat{T}_2 \hat{T}_3 \quad (3\text{-rd order}),
\end{aligned} \tag{10}$$


---

where we use a short-hand notation  $c_j = \cos(t_j/2)$ ,  $s_j = \sin(t_j/2)$ . We collect and explicitly label terms in Eq. (10) by orders of the formal parameter  $\lambda$  that can be attached to every  $\hat{T}_j$  and then set to 1 at the end of derivation [47]. In Eq. (10) one can recognize that products of generators at each order are terms of the elementary symmetric polynomial [48, Ch. 1.2] of that order. For example,  $\hat{T}_1 \hat{T}_2$ ,  $\hat{T}_1 \hat{T}_3$ , and  $\hat{T}_2 \hat{T}_3$  are terms of the elementary symmetric polynomial of the order 2 in three variables.

In a general case, Eq. (9), there are  $(M+1)$  groups corresponding to orders  $\lambda$  from 0 to  $M$ . Every elementary symmetric polynomial of the order  $K$  in  $M$  variables contains  $\binom{M}{K} = \frac{M!}{K!(M-K)!}$  terms, and a sum of them from  $K = 0$  to  $M$  gives  $2^M$  various products of  $M$  generators, again demonstrating the exponential complexity of the QCC form. Non-commutativity of generators has no consequences because of the condition  $i < j < k < \dots$  in the definition of the elementary symmetric polynomials (functions) [48, Ch. 1.2].

Grouping by orders of  $\lambda$  can be further exploited. After the factoring out the product of cosines of amplitudes  $\prod_{k=1}^M \cos(t_k/2)$  in Eq. (9), the amplitude-dependent coefficients in parentheses are the terms of elementary symmetrical polynomials in  $\tan(t_k/2)$ . If  $\forall k \tan(t_k/2) < 1$ , at every order the products of generators are multiplied by more quantities that are smaller than 1, so that their numerical contributions diminish. Broadly defining a weakly correlated regime as having all  $\tan(t_k/2) < 1$ , one may expect that keeping only groups from 0 to  $K < M$  in Eq. (9)

provides a fair approximation to the full expression.

The parenthesized expression in the last line of Eq. (9) can be interpreted as a rank decomposition of the operator-valued unitary  $\hat{U}(\mathbf{t}) = \hat{U}(t_1, t_2, \dots, t_M)$  of the rank  $M$  (as it depends on  $M$  “indices”  $t_i$ ) as a sum of lower-rank operators having the rank from  $K = 0$  to  $M$ . Rank decomposition is a powerful tool for investigating complex quantum systems, which is behind such approaches as the density-matrix renormalization group (DMRG) [49], or, more general, matrix product states (MPS) [50], and Tree Tensor Networks [51].

Let us denote  $\hat{U}^{[K]}(\mathbf{t})$  an approximation to the exact  $\hat{U}(\mathbf{t})$  in which all groups up to a  $K$ -th order in  $\lambda$  are kept. Then, an approximate energy functional *could be* defined as

$$W^{[K]}(\mathbf{t}) = \langle 0 | (\hat{U}^{[K]})^\dagger(\mathbf{t}) \hat{H} \hat{U}^{[K]}(\mathbf{t}) | 0 \rangle. \tag{11}$$

However, in general,  $W^{[K]}(\mathbf{t})$  is *not* variationally bound because  $\hat{U}^{[K]}(\mathbf{t})$  is not unitary unless  $K = M$ ,

$$\left( U^{[K]} \right)^\dagger U^{[K]} \neq \mathcal{E}, \quad K < M. \tag{12}$$

We anticipate poor quality of energies given by  $W^{[K]}(\mathbf{t})$  functional unless enough terms are retained. The upper-boundary property of Eq. (4), however, can be restored if we define

$$E^{[K]}(\mathbf{t}) = \frac{\langle 0 | (\hat{U}^{[K]})^\dagger(\mathbf{t}) \hat{H} \hat{U}^{[K]}(\mathbf{t}) | 0 \rangle}{\langle 0 | (U^{[K]})^\dagger(\mathbf{t}) U^{[K]}(\mathbf{t}) | 0 \rangle}, \tag{13}$$

which is our first, symmetric-polynomial approximate energy functional. Its implementation is reported in Appendix A.

It must be emphasized that neither  $W^{[K]}(\mathbf{t})$  nor  $E^{[K]}(\mathbf{t})$  coincide with an expression that follows from the expansion of the QCC *energy*, Eq. (3), either in the commutator or in perturbation-theory order [52].

## B. Limiting the expansion space

Formal algebraic independence of terms in Eq. (9) does not imply linear independence of individual terms in the *vector*  $\hat{U}(\mathbf{t})|0\rangle$ . Every contribution to  $\hat{U}(\mathbf{t})|0\rangle$  has a form  $\kappa_{\bar{q}}(\mathbf{t})\hat{T}_{\bar{q}}|0\rangle$ , where  $\hat{T}_{\bar{q}} = \hat{T}_{q_1} \cdots \hat{T}_{q_r}$ ,  $1 \leq r \leq M$  is a Pauli word and  $\kappa_{\bar{q}}(\mathbf{t})$  are functions of amplitudes. Any  $\hat{T}_{\bar{q}}$  can be uniquely factorized as

$$\hat{T}_{\bar{q}} = \phi_{\bar{q}} \hat{X}_{\bar{q}} \hat{Z}_{\bar{q}}, \quad (14)$$

where  $\phi_{\bar{q}} = \{\pm 1, \pm i\}$  is a factorization phase, and  $\hat{X}_{\bar{q}}$  and  $\hat{Z}_{\bar{q}}$  are some Pauli words that are products of only  $\hat{x}$  or  $\hat{z}$  Pauli elementary operators [*cf.* Eq. (2)], respectively. Because our reference state  $|0\rangle$  is an eigenvector of  $\hat{Z}_{\bar{q}}$  for

any  $\bar{q}$ :  $\hat{Z}_{\bar{q}}|0\rangle = f_{\bar{q}}|0\rangle$ ,  $f_{\bar{q}} = \pm 1$ , we can write

$$\hat{T}_{\bar{q}}|0\rangle = \phi_{\bar{q}} \hat{X}_{\bar{q}} \hat{Z}_{\bar{q}}|0\rangle = \phi_{\bar{q}} f_{\bar{q}} \hat{X}_{\bar{q}}|0\rangle. \quad (15)$$

Vectors (“excited states”)  $\hat{X}|0\rangle$  are linearly independent for different  $\hat{X}$ . It may occur, however, that different products of generators (*i.e.* with different  $\bar{q}$ ) factorize to the *same*  $\hat{X}$  operator, thus producing identical vectors albeit with different phases and different  $\kappa(\mathbf{t})$ . This coalescence of terms inevitably happen if  $M > n$  as it is not possible to generate more than  $2^n$  linearly independent vectors in the Hilbert space of dimensionality  $2^n$  (for  $n$  qubits).

The idea of approximating the vector  $\hat{U}(\mathbf{t})|0\rangle$  rather than the QCC unitary comes out naturally. This vector lives in a  $2^n$ -dimensional Hilbert space and evaluating and storing it on a classical computer is impossible for sufficiently large  $n$  and  $M$ . Hence, confining it in an  $N$ -dimensional subspace,  $N \ll 2^n$ , would be highly desirable. The main challenge is how to find a basis of that subspace, which, for example, maximizes the projection of  $\hat{U}(\mathbf{t})|0\rangle$  onto it.

Consider a step-by-step application of the unitary (5) to the reference vector  $|0\rangle$  [53]. Initially we have  $\mathbf{v}_0 = |0\rangle$  and  $\mathbf{V}_0 = \text{span}\{|0\rangle\}$ . Obviously,  $\mathbf{v}_0 \in \mathbf{V}_0$ . Then, applying exponents from the QCC unitary (5) starting from the rightmost factor  $\exp(-it_M \hat{T}_M/2)$ , we have:

$$\mathbf{v}_1 = \cos(t_M/2)\mathbf{v}_0 - i \sin(t_M/2)\hat{T}_M\mathbf{v}_0, \quad (16)$$

$$\begin{aligned} \mathbf{V}_1 &= \text{span}\{|0\rangle, -i\hat{T}_M|0\rangle\} \\ \mathbf{v}_2 &= \cos(t_{M-1}/2)\mathbf{v}_1 - i \sin(t_{M-1}/2)\hat{T}_{M-1}\mathbf{v}_1, \end{aligned} \quad (17)$$

$$\begin{aligned} \mathbf{V}_2 &= \text{span}\{|0\rangle, -i\hat{T}_M|0\rangle, -i\hat{T}_{M-1}|0\rangle, -\hat{T}_{M-1}\hat{T}_M|0\rangle\} \\ &\dots \end{aligned}$$

$$\mathbf{v}_k = \cos(t_{M-k+1}/2)\mathbf{v}_{k-1} - i \sin(t_{M-k+1}/2)\hat{T}_{M-k+1}\mathbf{v}_{k-1}, \quad (18)$$

$$\mathbf{V}_k = \text{span}\{|0\rangle, -i\hat{T}_M|0\rangle, \dots, -i\hat{T}_{M-k+1}|0\rangle, \dots, (-i)^k \prod_{j=k-1}^0 \hat{T}_{M-j}|0\rangle\}$$

$$2 < k \leq M$$

Here we use QCC generators multiplied by the factor  $(-i)$  because those products have purely real matrix elements in the computational basis set.

If no truncation is done up to the  $k$ -th level and no redundancy occurs, then  $\dim \mathbf{V}_k = 2^k$ . If, additionally,  $k = M$  then  $\dim \mathbf{V}_M = 2^M$  recovering the exponential complexity of the QCC unitary with respect to the number of generators. During this *expansion* stage the action of every exponential factor in the QCC unitary is represented exactly.

To suppress exponential growth the following strategy is followed: when the dimensionality of  $\mathbf{V}_k$  exceeds a

pre-defined number  $N$ , then  $(\dim \mathbf{V}_k - N)$  basis vectors which have the smallest absolute coefficients in  $\mathbf{v}_k$  are discarded, limiting the dimensionality of  $\mathbf{V}_k$  by  $N$ . After the application of the next exponential factor the size of  $\mathbf{V}_{k+1}$  cannot grow for more than  $2N$  (less if a coalescence of terms occurs), and analysis of  $\mathbf{v}_{k+1}$  is repeated limiting the dimensionality of  $\mathbf{V}_{k+1}$  by  $N$  as well. This is the *compression* stage. The process continues until all exponents in the QCC unitary are exhausted. At the end, one arrives at the final composition of the  $\mathbf{V}_M$  with  $\dim \mathbf{V}_M \leq N$  and finds the expansion coefficients of  $\mathbf{v}_M$  that are, in general, functions of all amplitudes.

TABLE I. The number of terms in  $\hat{U}^{[K]}(\mathbf{t})$  as a function of  $K$  and  $M = \dim \mathbf{t}$ . In the limiting case  $M = K$ , the number of terms is  $2^M$ ; if  $K \ll M$  it is  $O(M^K)$ .

$M \setminus K$	1	2	5	10	20
1	2	-	-	-	-
2	3	4	-	-	-
5	6	16	32	-	-
10	11	56	638	1024	-
20	21	211	21 700	616 666	1 048 576

If truncation happened at the  $k$ -th level, then the truncated vector  $\mathbf{v}_k$  has the norm less than one,  $\|\mathbf{v}_k\| < 1$ . This breaks the unitarity of the QCC Ansatz (5). We recover it by re-normalizing  $\mathbf{v}_k$  after truncating by rescaling its coefficients by  $1/\|\mathbf{v}_k\|$ . These re-normalization factors can be collected and stored to estimate the norm loss of the  $\hat{U}(\mathbf{t})|0\rangle$  during truncation.

Once properly normalized  $\mathbf{v}_M$  is computed, the approximate energy corresponding to the set of amplitudes  $\mathbf{t} = (t_1, t_2, \dots, t_n)$  can be evaluated as

$$F^{[N]}(\mathbf{t}) = \langle \mathbf{v}_M | H | \mathbf{v}_M \rangle \quad (19)$$

where expansion coefficients (“coordinates”) of  $\mathbf{v}_M$  in  $\mathbf{V}_M$  carry the information about the amplitudes. Equation (19) introduces our second approximate energy functional,  $F^{[N]}(\mathbf{t})$ . Its implementation is reported in Appendix B.

### C. General properties of the proposed energy functionals

Accuracy of  $E^{[K]}(\mathbf{t})$ , Eq. (13), and  $F^{[N]}(\mathbf{t})$ , Eq. (19), is controlled by the order parameter  $K \leq M$  and the expansion space dimensionality  $N \leq 2^{\min\{M,n\}}$ , respectively.

CPU and storage requirements for evaluating  $\hat{U}^{[K]}(\mathbf{t})$  rises steeply with  $K$  and  $M$  as

$$N(M, K) = \sum_{k=0}^K \binom{M}{k} = \sum_{k=0}^{\lfloor K/2 \rfloor} \binom{M+1}{K-2k}. \quad (20)$$

The last equality gives compact explicit expressions for  $K = 1$  and  $2$ :  $(M+1)$  and  $\frac{M(M+1)}{2} + 1$ , respectively. Numerical trends for other  $M$  and  $K$  are illustrated by Table I.  $E^{[K]}(\mathbf{t})$  provides energies and derivatives that are smooth with respect to variation of amplitudes. Contrary to that,  $F^{[N]}(\mathbf{t})$  is, in general, *non-differentiable* as the composition of the truncated space can be drastically different for close but distinct values of input amplitudes, leading to non-smooth variation of energies with respect to  $\mathbf{t}$ , with an exception of the limiting case  $N = 2^{\min\{M,n\}}$ . Thus,  $F^{[N]}(\mathbf{t})$  is less suitable for amplitude optimization than  $E^{[K]}(\mathbf{t})$ .

### D. Diagonal Hessian approximation (DHA) and new generator ranking

$E^{[K]}(\mathbf{t})$  for  $K = 1$  can be simplified further. Consider

$$\begin{aligned} \hat{U}^{[1]}(\mathbf{t}) &= \prod_{k=1}^M \cos(t_k/2) \left( 1 - i \sum_{j=1}^M \tan(t_j/2) \hat{T}_j \right) \\ &= \mathcal{R}_M(\mathbf{t}) \left( 1 - i \sum_{j=1}^M C_j \hat{T}_j \right), \end{aligned} \quad (21)$$

where we defined

$$\mathcal{R}_M(\mathbf{t}) = \prod_{k=1}^M \cos(t_k/2), \quad (22)$$

$$C_j = \tan(t_j/2). \quad (23)$$

From Eq. (13)  $E^{[1]}(\mathbf{t})$  is then

$$\begin{aligned} E^{[1]}(\mathbf{t}) &= \left( 1 + \sum_{k=1}^M C_k^2 \right)^{-1} \left( 1 - i \sum_{k=1}^M C_k \langle 0 | [\hat{H}, \hat{T}_k] | 0 \rangle + \sum_{j,k=1}^M C_j C_k \langle 0 | \hat{T}_j \hat{H} \hat{T}_k | 0 \rangle \right) \\ &= \left( 1 + \sum_{k=1}^M C_k^2 \right)^{-1} \left( 1 + 2 \sum_{k=1}^M C_k g_k + \sum_{j,k=1}^M C_j C_k \langle 0 | \hat{T}_j \hat{H} \hat{T}_k | 0 \rangle \right), \end{aligned} \quad (24)$$

because  $\langle 0 | \hat{T}_j \hat{T}_k | 0 \rangle = \delta_{jk}$  (the Kronecker delta). We also used the definition of QCC energy gradients  $g_k$ , Eq. (6).

Minimization of  $E^{[1]}(\mathbf{t})$  with respect to  $\mathbf{C} = C_1, C_2, \dots$  [see Eq. (23)] leads to the standard eigenvalue problem for the *Hessian* matrix  $\mathbf{H}$ ,

$$\mathbf{H}\mathbf{C} = \mathbf{E}\mathbf{C}. \quad (25)$$

Minimization with respect to amplitudes  $\mathbf{t}$  rather than  $\mathbf{C}$  by demanding

$$\frac{\partial E^{[1]}(\mathbf{t})}{\partial t_j} = \sum_k \frac{\partial E^{[1]}(\mathbf{C})}{\partial C_k} \frac{\partial C_k}{\partial t_j} = 0 \quad (26)$$

leads to the *same* minimum, since the Jacobian of trans-

formation,  $\left\{ \frac{\partial C_k}{\partial t_j} \right\} = \text{diag} \left\{ \frac{\partial C_j}{\partial t_j} \right\} = \text{diag} \left\{ \frac{1}{2 \cos^2(t_j/2)} \right\}$  is singular only if  $\cos(t_j/2) = 0$  for some  $j$ . In this case, one of the rotated states,  $\hat{T}_j |0\rangle$ , [see Eq. (8)] is orthogonal to the reference state  $|0\rangle$ , which implies reference *instability*. We assume this situation never occurs.

The diagonal Hessian approximation (DHA) is introduced by ignoring all the off-diagonal ( $j \neq k$ ) terms in the last sum in Eq. (24), which implies the following structure of the  $(M+1) \times (M+1)$  Hessian matrix:

$$\mathbf{H} = \begin{pmatrix} E_0 & g_1 & g_2 & \cdots & g_M \\ g_1 & E_1 & 0 & \cdots & 0 \\ g_2 & 0 & E_2 & & 0 \\ \vdots & \vdots & & \ddots & \vdots \\ g_M & 0 & \cdots & & E_M \end{pmatrix}, \quad (27)$$

where  $E_0 = \langle 0 | \hat{H} | 0 \rangle$  is the reference energy,  $g_k$  are QCC gradients, and

$$E_k = \langle 0 | \hat{T}_k \hat{H} \hat{T}_k | 0 \rangle = \langle 0 | \hat{X}_k \hat{H} \hat{X}_k | 0 \rangle, \quad k = 1 \dots M \quad (28)$$

are the excited-state energies. Equation (28) uses Eq. (15) to get rid of phase factors and refer to unique basis states  $\hat{X}_k |0\rangle$ .

The ground-state eigenvalue (energy)  $E$  and the corresponding amplitudes  $\mathbf{t} = 2 \arctan(\mathbf{C})$  for the eigenproblem (25) with the matrix (27) can be found via an iterative procedure. In fact,  $E$  is identical to the energy given by the Brillouin–Wigner perturbation theory [54, 55] for the state  $|0\rangle$ .

Because the optimal amplitudes in DHA can be efficiently found even for  $\dim \mathbf{t} = M \gtrsim 10^8$ , the absolute values  $|t_k|$  can be used for *ranking* generators—to include the top-ranked ones into the QCC Ansatz. This is a new alternative to the ranking schemes proposed in Ref. 56, see Sec. III B.

### III. SIMULATIONS DETAILS

#### A. General setup

The active-space fermionic Hamiltonians for these molecules are written in the spin-orbital basis and converted to a qubit form using the JW transformation. Spin-orbitals are grouped as  $\phi_1 |\alpha\rangle, \phi_1 |\beta\rangle, \phi_2 |\alpha\rangle$ , etc, where  $\phi_i$  are the restricted Hartree–Fock (RHF) *spatial* orbitals and  $|\alpha\rangle$  and  $|\beta\rangle$  are spin-1/2 eigenfunctions. RHF molecular orbitals (MOs) generation and the atomic orbital (AO) to MO transformation for the active spaces were done using the modified version of the GAMESS [57, 58] program suit. Active-space configuration interaction singles and doubles (CISD), coupled-cluster singles and doubles (CCSD), and complete active space configuration interaction (CASCI) calculations for the N<sub>2</sub> molecule were done in Psi4 [59] program package, version 1.3.1, while CISD, CISDT, CISDTQ, CCSD and coupled-cluster singles and doubles and

non-iterative triples (CCSD(T)) active-space energies for Ir(F<sub>2</sub>ppy)<sub>3</sub> were calculated in GAMESS. Preparing qubit Hamiltonians and iQCC iterations are performed by a proprietary suit of programs written in JULIA [60] language. Energy minimization was always performed with L-BFGS algorithm [61, 62] implemented in the NLOpt [63] JULIA package.

#### B. Generator ranking

Generators included into the QCC Ansatz were ranked by the formula [56]:

$$r_j = \left| \arcsin \frac{2g_i}{\sqrt{D_i^2 + 4g_i^2}} \right| = \left| \arctan \frac{2g_i}{D_i} \right|, \quad (29)$$

where  $g_i$  is the gradient associated with a candidate generator  $\hat{T}_i$  [see Eq. (6)] and  $D_i = \langle 0 | \hat{H} | 0 \rangle - \langle 0 | \hat{T}_i \hat{H} \hat{T}_i | 0 \rangle = E_0 - E_i$  is a difference between the reference energy  $E_0$  and the excited state energies  $E_i$ , see Eq. (28). In the limit of small couplings  $g_i \ll D_i$  this formula is reduced to the Epstein–Nesbet [64, 65] perturbation-theory expression for the first-order absolute amplitudes,  $|2g_i/D_i|$ . Equation (29), however, provides robust ranking even in the case of strong correlation when  $D_i \ll g_i$ , and a perturbation theory fails.

## IV. RESULTS AND DISCUSSION

#### A. Dinitrogen (N<sub>2</sub>, 16 qubit)

For the N<sub>2</sub> molecule we performed RHF calculations using Dunning’s cc-pVDZ basis set [66]. The complete active space (CAS) included all 8 valence (comprised of 2s and 2p orbitals of both N atoms) RHF MOs and 10 valence electrons; it is CAS(10, 8). The 16-qubit Hamiltonian was produced as described in Sec. III. It contains 825 terms larger than  $10^{-8}$  in magnitude and has 136 generators, which correspond to single and double fermionic excitations, with potentially non-zero gradients (6). Some of them, however, have numerically zero gradients for the closed-shell Hartree–Fock reference with 8 electrons, for example those that correspond to the occupied-occupied or virtual-virtual excitations. On the other hand, including them to the QCC Ansatz makes it similar to the disentangled form of generalized unitary coupled cluster singles and doubles (GUCCSD) method [17] or a unitarized version of the iterative n-body excitation inclusive coupled-cluster single double (iCCSDn) theory [41].

First, we study the convergence of  $E^{[K]}$ , Eq. (13), with respect to  $K$  for the case of weak correlation. The weakly correlated case is represented by the N<sub>2</sub> molecule with  $d(N–N) = 2.118 a_0$ , which is close to the equilibrium geometry at the full configuration interaction (FCI) level in the cc-pVDZ basis. At this internuclear distance the singlet ground state of the molecule is well-separated from

TABLE II. N<sub>2</sub> molecule with d(N–N) = 2.118  $a_0$ . The optimal energies  $E_{\text{opt}}^{[K]}$ , exact energies at optimized amplitudes  $E(\mathbf{t}_{\text{opt}}^{[K]})$ , and the norm of deviation  $\|\mathbf{t}_{\text{opt}}^{[K]} - \mathbf{t}_{\text{exact}}\|$  along with the number of terms in  $\hat{U}^{[K]}(\mathbf{t})$  and the length (dimensionality) of  $\hat{U}^{[K]}(\mathbf{t})|0\rangle$  for  $K$  from 0 to  $M = 22$ .  $\mathbf{t}_{\text{exact}}$  are the amplitudes optimized for  $K = M$ . A special case  $K = 0$  corresponds to the amplitudes optimized using DHA, see Sec. IID.

$K$	Terms in $\hat{U}^{[K]}(\mathbf{t})$	dim ( $\hat{U}^{[K]}(\mathbf{t}) 0\rangle$ )	$E_{\text{opt}}^{[K]}$	$E(\mathbf{t}_{\text{opt}})$	$\ \mathbf{t}_{\text{opt}} - \mathbf{t}_{\text{exact}}\ $
0	23	23	-109.058174408	-109.011843381	$2.25 \times 10^{-1}$
1	23	23	-109.027206664	-109.027501062	$6.59 \times 10^{-2}$
2	254	146	-109.028505327	-109.028475415	$5.66 \times 10^{-3}$
3	1794	438	-109.028482438	-109.028483240	$6.06 \times 10^{-4}$
4	9109	764	-109.028483783	-109.028483322	$4.76 \times 10^{-5}$
5	35443	956	-109.028483312	-109.028483322	$1.69 \times 10^{-6}$
6	110056	1016	-109.028483323	-109.028483322	$1.01 \times 10^{-7}$
7	280600	1024	-109.028483322	-109.028483322	$7.06 \times 10^{-8}$
8–22	Eq. (20)	1024	-109.028483322	-109.028483322	$7.19 \times 10^{-8}$
Exact				-109.028483322	0

higher-spin states, and iQCC iterations converge eventually to the exact ground-state singlet energy. We consider only the first iteration when  $E^{[K]}$  is optimized using the fermionic Hamiltonian  $\hat{H}^{(0)}$  [c.f. Eq. (7)]. Generators were ranked by Eq. (29), and we selected  $M = 22$  of them; this value is close to the limit of optimization of un-truncated  $\hat{U}(\mathbf{t})$  due to CPU and memory limitations of a typical workstation.

The optimized energies  $E_{\text{opt}}^{[K]}$ , exact energies at the optimized amplitudes  $E(\mathbf{t}_{\text{opt}}^{[K]})$ , the norm of deviation  $\|\mathbf{t}_{\text{opt}}^{[K]} - \mathbf{t}_{\text{exact}}\|$  along with the number of terms in  $\hat{U}^{[K]}(\mathbf{t})$  and the length (dimensionality) of  $\hat{U}^{[K]}(\mathbf{t})|0\rangle$  for  $K = 1$  to  $M$  are shown in Table II.  $\mathbf{t}_{\text{exact}}$  are the amplitudes optimized for  $K = M$ . A special case labelled by  $K = 0$  corresponds to the optimization in the DHA approximation, see Sec. IID. As follows from the Table II, the optimized energies and amplitudes converge quickly with increasing of  $K$ : sub-millihartree accuracy is already achieved at  $K = 2$ , and a numerically converged result can be obtained for  $K = 6$ . The norm of deviation  $\|\mathbf{t}_{\text{opt}}^{[K]} - \mathbf{t}_{\text{exact}}\|$  decreases roughly by an order of magnitude each time  $K$  increases by 1 until  $K = 7$ , and then stalls because the numerical precision of the objective function (energy) is limited by its float-point representation on a computer. Overall, these results emphasizes the fact that in a weakly correlated system the exact representation of a system wave function is highly redundant because of the dominance of vanishing numerical contributions [67].

Secondly, we investigate convergence of of  $E^{[K]}(\mathbf{t})$ , Eq. (13), with respect to  $K$  for the case of strong correlation represented by a stretched N<sub>2</sub> molecule with d(N–N) = 4.0  $a_0$ . At this nuclear configuration the singlet ground state is highly multiconfigurational. The configuration interaction (CI) coefficient of the Hartree–Fock reference is approximately 0.5. IQCC iterations in this case converge to a superposition of ground and higher-multiplicity states. Fundamentally, this happens because some of generators are not spin-adapted and contribute

to the creation of both open-shell singlet and  $S_z = 0$  components of triplets. In this case energy optimization suffers from strong spin contamination and, unless constrained optimization techniques or penalties [45, 68] are employed, the spin symmetry breaking is almost unavoidable. Ultimately, this is reminiscent Löwdin symmetry dilemma [69], which plagued the Hartree–Fock optimization of singlet states in the spin-unrestricted formalism. For the sake of demonstration, we did *not* add penalty operators to the Hamiltonian, but tracked the mean value of  $\hat{S}^2$  operator computed at the set of optimized amplitudes. Additionally, in this case we used  $M = 19$  to avoid cutting the group of generators with almost identical values of ranking—such a precaution measure is necessary to prevent *artificial* symmetry breaking.

The convergence of  $E_{\text{opt}}^{[K]}$  and related quantities are reported in Table III. Unsurprisingly,  $E^{[K]}$  struggles to obtain the correct solution for  $K$  up to 3. Starting from  $K = 4$  onward, amplitudes converge geometrically with increasing  $K$ , lowering the norm of the difference with the exact amplitudes by roughly one order of magnitude per unit step. It is clear also that optimization without constraints/penalties has a tendency to converge to the high-spin solution rather than a singlet—this can be seen from expectation values of the total spin-squared operator  $\hat{S}^2$ . Energy is converged to sub-millihartree accuracy at  $K = 4$ , but the mean value of  $\hat{S}^2$  roughly stabilises at  $K = 5$ . Thus, in the strongly-correlated case convergence with respect to  $K$  is slower, suggesting  $K > 4$  for accurate optimization. Consequently, numerical efforts for energy optimization exhibit relatively steep scaling,  $O(M^5)$  or worse. It should be taken into account, however, that in this case it would be more prudent not to try optimization of a large number of generators at once, but instead combine generators in groups, optimizing the mostly important (strongly correlated) first and rely on the iterative iQCC procedure. Only in extremely pathological cases—like the full dissociation of a covalent crystal—a strongly correlated subsystem will have more than a few dozens of

TABLE III. N<sub>2</sub> molecule with d(N–N) = 4.0  $a_0$ . The optimal energies  $E_{\text{opt}}^{[K]}$ , exact energies at optimized amplitudes  $E(\mathbf{t}_{\text{opt}}^{[K]})$ , the norm of deviation  $\|\mathbf{t}_{\text{opt}}^{[K]} - \mathbf{t}_{\text{exact}}\|$ , and the expectation value for the total spin-squared operator  $\langle \hat{S}^2(\mathbf{t}_{\text{opt}}) \rangle$  along with the number of terms in  $\hat{U}^{[K]}(\mathbf{t})$  and the length (dimensionality) of  $\hat{U}^{[K]}(\mathbf{t})|0\rangle$  for K from 0 to M = 19.  $\mathbf{t}_{\text{exact}}$  are the amplitudes optimized for K = M. A special case K = 0 corresponds to the amplitudes optimized using DHA, see Sec. II D.

K	Terms in $\hat{U}^{[K]}(\mathbf{t})$	dim $\hat{U}^{[K]}(\mathbf{t}) 0\rangle$	$E_{\text{opt}}^{[K]}$	$E(\mathbf{t}_{\text{opt}})$	$\ \mathbf{t}_{\text{opt}} - \mathbf{t}_{\text{exact}}\ $	$\langle \hat{S}^2(\mathbf{t}_{\text{opt}}) \rangle$
0	20	20	-108.8586872116	-108.5895989786	2.4	0.065012
1	20	20	-108.6050091792	-108.1867637296	2.3	0.820330
2	191	87	-108.6961743172	-108.6242746563	$8.3 \times 10^{-1}$	2.162786
3	1160	128	-108.7219620714	-108.7152274369	$4.6 \times 10^{-1}$	2.068216
4	5036	128	-108.7266865097	-108.7261532367	$2.6 \times 10^{-1}$	2.082183
5	16664	128	-108.7268735613	-108.7267206541	$3.9 \times 10^{-2}$	2.144843
6	43796	128	-108.7267755035	-108.7267551552	$5.1 \times 10^{-3}$	2.154885
7	94184	128	-108.7267564062	-108.7267562398	$8.0 \times 10^{-4}$	2.153763
8	169766	128	-108.7267564209	-108.7267562538	$6.9 \times 10^{-5}$	2.153521
9	262144	128	-108.7267562453	-108.7267562539	$3.5 \times 10^{-6}$	2.153535
10–19	Eq. (20)	128	-108.7267562539	-108.7267562539	$O(10^{-7})$	2.153534
Exact				-108.7267562539	0	2.153534

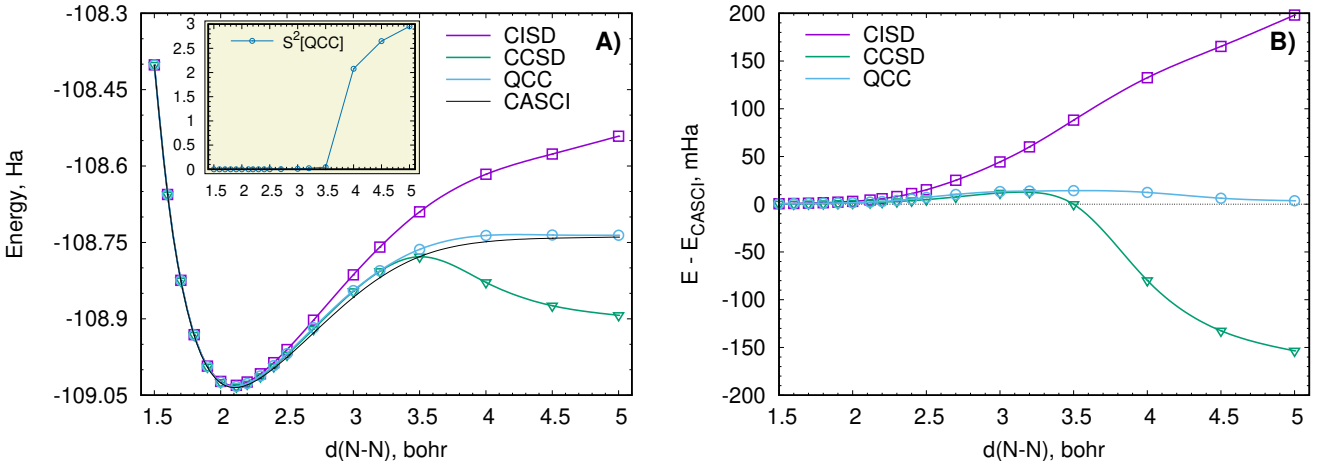
generators.

Finally, we computed the PEC for the range d(N–N) = 1.5–5.0  $a_0$  with the full set of potentially non-zero generators, M = 136; see Fig. 1. Optimization of the QCC energy with the exact QCC Ansatz (5) with M = 136 on a classical computer is out of the question: the un-truncated  $\hat{U}(\mathbf{t})$  contains  $2^{136} \approx 8.7 \times 10^{40}$  terms. Low-order expansions with  $K \leq 4$  are tractable, but optimal energies will not be exact. However, for a 16-qubit system, the dimensionality of the qubit Hilbert space is no greater than  $2^{16} = 65\,536$ . Moreover, since the second-quantized Hamiltonian also carries information about states with different number of electrons, spins, *etc.*, its matrix representation has a block-diagonal form, with blocks that couple only the states with the same number of electrons (Hamiltonian is particle-conserving), same spin (we consider systems in the absence of a magnetic field and ignore spin-orbit coupling), and—if a system possesses spatial symmetry—belonging to the same irreducible representation of the corresponding symmetry group. Not all symmetries can be simply accounted for in the qubit representation. The so-called qubit tapering technique [70, 71] allows for reducing the dimensionality of Hilbert space by 5 qubits for systems possessing  $D_{\infty h}$  symmetry; hence, the symmetry-reduced Hamiltonian for the state of a particular symmetry, namely, 10-electron singlet  $A_{1g}$  state, will be characterized by only  $16 - 5 = 11$  qubits, and the corresponding qubit Hilbert space dimensionality is merely  $2^{11} = 2048$ . This opens up a possibility to find the exact QCC energy using the functional  $F^{[N]}(\mathbf{t})$ , Eq. (19), with  $N = 2048$ . Our  $F^{[N]}(\mathbf{t})$  implementation (see Sec. B) automatically detects that the number of unique  $\hat{X}|0\rangle$  states is no greater than 2048. It is also notable that the dimensionality of invariant subspaces depends on the set of generators too. As follows from Table II, for M = 22 generators ranked by Eq. (29) the size of the invariant subspace is 1024, while in the case of stretched molecule

and M = 19 it is merely 128, see Table III.

Another salient feature of the QCC Ansatz is its order-dependence, which is common among other VQE methods [38, 72–74]. This *ordering problem* has the fundamental consequences, such as whether the particular ordering guarantees the exact solution or not [38], or can significantly impact on shapes of PECs [72]. In the QCC Ansatz the order of generators is determined by the ranking scheme; see Sec. IIIB. Unfortunately, ordering of generators with numerically close or identical ranking values can still be affected by uncontrollable numerical noise. We solved this issue by first assuming that generators are *degenerate* if their ranking values rounded to  $10^{-11}$  are identical. These degenerate generators, in turn, were ordered according to the binary representation of their  $\hat{X}$  factors, see Eq. (14), thus completely fixing ambiguity. It must be noted that the ordering problem in the *iterative* approach (complete iQCC) is virtually non-existent: the method will eventually converge to a FCI or CASCI value (which is unique) albeit with slightly different rates.

In Fig. 1 we also show PECs computed by conventional quantum chemistry methods: the CISD, CCSD, and CASCI ones; all of them used the same active space, CAS(10, 8). For the range of N–N distances where correlation is weak-to-moderate (1.5–2.5  $a_0$ ), both CCSD and QCC methods agree very well with the CASCI reference and each other: deviations from the CASCI energy do not exceed 10 mE<sub>h</sub>. The CCSD method is consistently closer to the CASCI reference than QCC, but this could be explained by its non-variational nature. Starting from d(N–N) = 3.5  $a_0$  the quality of estimates given by CCSD and, especially, the CISD method quickly deteriorates while the QCC method performs noticeably better: its deviation from CASCI does not exceed 15 mE<sub>h</sub>. However, the apparent quality of the QCC energies is not confirmed by quality of underlying wave function: form the inset in Fig. 1A it is clear that the QCC wave func-

FIG. 1. Potential energy curves for  $\text{N}_2$ .

tion becomes strongly spin-contaminated starting from  $d(\text{N}-\text{N}) = 3.5 a_0$ : the mean value of  $\hat{S}^2$  operator jumps from essentially zero to almost 3 at  $5.0 a_0$ . This is another manifestation of Löwdin's symmetry dilemma [69] but for the correlated wave function.

In general, the QCC method with the full set of generators provides energies that are considerably better than CISD ones and close to the results of CCSD method when correlation is not too strong. QCC energy estimates also demonstrate robustness to changes in the electronic structure of a system of interest. Overall, the QCC method is similar to the disentangled (factorized) unitary coupled cluster (UCC) method [38, 39, 75], which uses different form of generators.

### B. Water molecule ( $\text{H}_2\text{O}$ , 36 qubits)

Preparatory calculations were the following. We have performed RHF calculations using Pople's 6-31G(d) basis set [76] for a near-equilibrium molecular configuration,  $d(\text{O}-\text{H}) = 0.95 \text{ \AA}$ . The valence  $\angle \text{HOH}$  was fixed at  $107.6^\circ$ . The CAS was formed by taking all RHF MOs except the lowest-energy one, which correlates with core 1s orbital of the O atom, resulting in CAS(8, 18). The 36-qubit Hamiltonian, prepared as described in Sec. III A, contained 41 907 terms greater than  $10^{-8}$  in magnitude.

In this example we examined the use of  $F^{[N]}(\mathbf{t})$ , Eq. (19), for energy extrapolation when the exact QCC energy is unattainable. The 36-qubit Hamiltonian has 7929 groups associated with all possible single and double excitations—this is the total number of generators which satisfy non-zero gradient criterion, Eq. (6). As was already noted above, some of them (for example, single and double virtual-virtual vv/vvv excitation) are associated with numerically zero gradients for the 8-electron singlet reference state. To simplify our task, we retained only single and double excitations of ov and oovv types. Since gradients of the ov-type excitations are very small because

TABLE IV. Convergence of  $F^{[N]}(\mathbf{t})$ , Eq. (19), with respect to the size of the expansion space  $N$ . Amplitudes are optimized with  $E^{[2]}(\mathbf{t})$  energy expression, Eq. (13); the optimized energy value is  $-76.196411$ . Timings are collected for 48-thread execution on an AMD EPYC 24-core processor with 2 TB of RAM.

$N$	Energy, $E_h$	Time, s
262 144	-76.1962776	213
524 288	-76.1962569	559
1 048 576	-76.1962433	1634
2 097 152	-76.1962345	5259
4 194 304	-76.1962307	18 315
8 388 608	-76.1962299	67 353
16 777 216	-76.1962297	249 700
33 554 432	-76.19622961	958 630

of using the Hartree–Fock orbitals, all included generators are naturally arranged “doubles first, singles last” [38], leading to the QCC Anzatz with  $M = 1182$  generators.

We estimate the dimensionality of the 36-qubit Hilbert space that contains the exact ground state as  $2^{32} = 4\ 294\ 967\ 296$  because the qubit tapering technique [70, 71] allows for reducing the dimensionality of Hilbert space by 4 qubits for the system with  $C_{2v}$  symmetry. Thus, the exact solution can be obtained with  $F^{[N]}(\mathbf{t})$  for  $N = 4\ 294\ 967\ 296$ , which is currently impossible in our implementation. Instead, we assessed the following scheme: first, we optimize amplitudes with  $E^{[K]}(\mathbf{t})$  for  $K = 2$ . Despite of not being fully convergent, they might be a fair approximation to the exact result, especially for the weakly correlated case. Next, we calculate a sequence of energies with  $F^{[N]}(\mathbf{t})$  using these amplitudes and values of  $N$  ranging from  $2^{18} = 262\ 144$  to  $2^{25} = 33\ 554\ 432$  with the ratio of 2; see Table IV. From the results in Table IV it is clear that we have achieved sub- $\mu E_h$  convergence of the total energy already at  $N = 2^{24} = 16\ 777\ 216$ , which is only 0.4% of the full Hilbert space dimensionality. As was anticipated for the weakly correlated case, the exact energy estimate is close to the optimized  $E^{[2]}(\mathbf{t})$  energy.

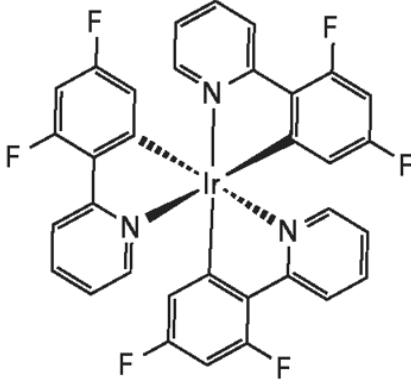


FIG. 2. Tris[2-(2,4-difluorophenyl)pyridine]iridium(III)

Timings demonstrate a transition from a linear-scaling evaluation of the expansion vector to a quadratic regime associated with energy evaluation via vector-matrix multiplication. Expansion vector is computed on a single thread, while the matrix-vector multiplication can utilize all available cores, so that using more cores will effectively reduce elapsed (“wall-clock”) time.

### C. Large-scale (80 qubits) iQCC calculations for $\text{Ir}(\text{F}_2\text{ppy})_3$ and energy extrapolation with $E^{[1]}(\mathbf{t})$ .

To demonstrate scalability of our symmetric polynomial-based optimizer and integrate it into the iQCC workflow, we have performed a singlet ground-state energy optimization for one of the typical organic light-emitting diode (OLED) materials, tris(2-(2,4-difluorophenyl)pyridine)iridium(III),  $\text{Ir}(\text{F}_2\text{ppy})_3$ ; see Fig. 2. Its 80-qubit Hamiltonian  $\hat{H}^{(0)}$  [77], containing 3 532 677 terms that are larger than  $5 \times 10^{-7}$  in magnitude was prepared as follows. First, we performed RHF calculations on that molecule using the 6-31G(d) basis set on light atoms (H, C, N, and F), and SBKJC pseudopotential + DZ valence basis set [78] on Ir. 6-component (Cartesian)  $d$  harmonics were used throughout. The converged Hartree–Fock energy for the lowest singlet  $S_0$  state was  $-2124.157\,531 E_h$ . 20 occupied RHF MOs along with 20 virtual RHF orbitals that are closest to the Fermi level formed CAS(40, 40), from which we generate the qubit expression as described in Sec. III.

We have executed seven iQCC iterations with 10, 50, 50, 50, 50 and 200 000 generators ranked according to the measure (29), optimizing  $E^{[K]}(\mathbf{t})$  energy expression with  $K = 10, 3, 3, 3, 3$  and 1, respectively. All the steps except the last one involved dressing of the current Hamiltonian by Eq. (7) and dropping the terms that are smaller than  $5 \times 10^{-7}$  in magnitude. The size of the (dressed) Hamiltonian at the final 7-th iteration was 620 228 571 terms. Choosing 10 generators at the first iteration allowed us to include a group of spin-preserving generators

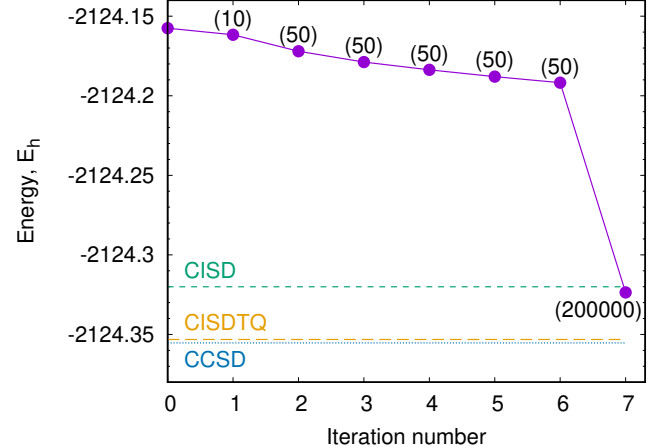


FIG. 3. Convergence of iQCC iterations for  $\text{Ir}(\text{F}_2\text{ppy})_3$ . The zeroth iteration shows the initial RHF energy,  $-2124.157\,531 E_h$ . The numbers in parenthesis are the number of generators used at the corresponding iteration.

and decrease the maximum ranking value from 0.0611 to 0.0453 without spin symmetry breaking. At all subsequent iterations the wave function becomes progressively spin-contaminated, with  $\langle S^2 \rangle$  value reaching 0.0287 at the 7-th iteration, while the maximum ranking value decreased to 0.0205. Our final iQCC variational energy estimate after amplitude optimization with 200 000 generators was  $-2124.323\,570 E_h$ . This value should be compared to the CISD, CISDTQ, and CCSD energies computed for the same active space, see Fig. 3. The iQCC method provides energies below the variational CISD estimate, but disconnected quadruple contributions that are mostly responsible for the difference between CISD and CISDTQ/CCSD estimates (connected triples contributions are small, of the order of  $\approx 0.002 E_h$ ) are not well-captured at  $K = 1$  level. Overall, for this weakly-correlated system the variational CISDTQ estimate should be rather close to the exact CASCI value.

Timings for the amplitude optimization are shown in Table V. It is clear that even with a large number of generators, timings for the amplitude optimization with our new optimizer are rather modest.

We also compare our optimizer with Amazon’s sparse

TABLE V. Timings for the singlet ground-state energy minimization for  $\text{Ir}(\text{F}_2\text{ppy})_3$ . 24-thread execution on an AMD EPYC 24-core processor with 2 Tb of RAM.

Iteration \ Hessian + amplitude optimization, s
1 $3.1 + 2.5 = 5.6^1$
2 $2.3 + 0.5 = 2.8$
3 $10.1 + 1.6 = 11.7$
4 $16.8 + 0.1 = 16.9$
5 $25.2 + 6.5 = 31.7$
6 $38.1 + 10.1 = 48.2$
7 $3509 + 80970 = 84\,479$

<sup>1</sup> Including time for JULIA JIT compilation [60].

TABLE VI. Comparison of the current energy/amplitude optimizer with with Amazon's sparse wave function simulator (AWS) [46].

	$E^{[K]}(\mathbf{t})$	AWS
Final energy, $E_h$	-2124.323 570	-2124.225 246
Generators used	200 110	1100
Total simulation time, s	119 221	56 071
Number of CPUs	24	96
CPU time, h	563.2	1495.2

wave function simulator (AWS) [46]. AWS used `r7i.metal-48x1` Amazon EC2 instance. An instance is a two-socket computer with Intel(R) Xeon(R) Platinum 8488C CPUs, each with 48 cores and two threads per core. Timings as well as other relevant quantities are summarized in Table VI.

We would like to emphasize that the total time reported for the iQCC method contains many other steps that are not performed by the AWS; the corresponding breakdown of the total time is given in Table VII.

## V. CONCLUSIONS

The QCC Ansatz (5) with  $M$  generators that lies at the heart of the iQCC method is exponentially hard for classical computers. To make it more amicable to classical hardware, we propose two approximations for the QCC energy expression (3):  $E^{[K]}(\mathbf{t})$ , Eq. (13) and  $F^{[N]}(\mathbf{t})$ , Eq. (19). The first one,  $E^{[K]}(\mathbf{t})$ , is based on the symmetric polynomial expansion of the exact expression up to the specified order  $1 \leq K \leq M$ . We have demonstrated that the optimal energy and amplitudes obtained with  $E^{[K]}(\mathbf{t})$  converge geometrically with increasing  $K$ . The onset of the geometrical convergence depends on a system under consideration: for weakly correlated systems chemically accurate energies can be obtained with  $K = 2$  and microhartree accuracy can be achieved already at  $K = 3$ . For strongly correlated systems the convergence is somewhat delayed, but microhartree accuracy can be obtained at  $K = 6$ . The value  $K = 4$  is recommended for expedite calculations with the chemical accuracy ( $\leq 1 \text{ m}E_h$ ) in the case of strong correlation. For any  $K$ ,  $E^{[K]}(\mathbf{t})$  is a differentiable expression with continuous gradients which are necessary for applying efficient gradient-based optimization algorithms, such as L-BFGS [61]. Remarkably,  $E^{[K]}(\mathbf{t})$  for  $K = 1$  is equivalent to a linear parametrisation of a

TABLE VII. The total simulation time breakdown for the iQCC method; only rate-limiting steps are shown.

Step	Time, s
Hamiltonian dressing	27 554
Hessian + amplitude optimization	84 596
<b>Total<sup>1</sup></b>	112 151

<sup>1</sup> Auxiliary calculations contribute to the difference with the total execution time reported in Table V.

correlated wave function, known as the CI expansion in the traditional quantum chemistry with the mapping of CI expansion coefficients to cluster amplitudes via Eq. (23). CI-like expansion can be optimized with hundreds of thousands of generators, which we exploited to extrapolate the energies to the CASCI limit, see Sec. IV C.

Continue along the line of simplification, we have introduced the diagonal Hessian approximation (DHA) (see Sec. II D) that is based on  $E^{[1]}(\mathbf{t})$ , which can be used not only as an extrapolation technique allowing for including hundreds of millions generators, but also for ranking them, thus defining an alternative to “first-order unitary ranking” discussed in Sec. III B.

The main obstacle with  $E^{[K]}(\mathbf{t})$  is steep scaling of computational efforts with increasing  $M$  and  $K$  as  $O(M^K)$  for  $K \ll M$ ; see Eq. (20) and Table I. To address this issue we introduced our second energy expression  $F^{[N]}(\mathbf{t})$ , Eq. (19), where  $N$  is the dimensionality of the expansion space—in other words, the number of “qubit excited states”. The latter—the number of qubit product states for  $n$  qubits—is fundamentally limited by the size of the corresponding Hilbert space,  $2^n$ , but in the most of practically relevant cases  $n \gg 30$  ( $\sim 15$  active orbitals), and the limit is unattainable. However, as is established in the CI theory [67], much fewer states may be needed for chemically accurate total energies. To test this assertion, we performed a convergence study of  $F^{[N]}(\mathbf{t})$  for increasing  $N$ . In the particular case of 36-qubit  $\text{H}_2\text{O}$  Hamiltonian, for which we estimate the size of the relevant Hilbert space as  $N_{\text{lim}} = 2^{32}$ ,  $F^{[N]}(\mathbf{t})$  energies for  $N = 2^{24} \approx 0.4\%$  of  $N_{\text{lim}}$  appear to converge to  $\mu E_h$  accuracy. Despite its flexibility and computational efficiency,  $F^{[N]}(\mathbf{t})$  is less suitable for optimization, because it encodes, in general, a non-smooth function of amplitudes as the composition of the expansion space can drastically change even for close but distinct amplitude vectors  $\mathbf{t}$ .

In the first time we have calculated the entire PEC for the  $\text{N}_2$  molecule using the QCC Ansatz with all possible generators satisfying the non-zero gradient criterion (6). Our results suggest that the QCC form is an alternative to the disentangled/factorized form of the UCC method [38, 39, 41, 75] whose generators are derived from fermion single- and double-excitation operators. An important advantage of QCC generators is that they not need to be derived from any fermionic predecessors, which ultimately leads to the iterative scheme realized as the iterative qubit coupled cluster (iQCC) method [34].

Fundamentally, we have demonstrated that the maximum possible entanglement that may be provided by a noise-free quantum computer is hardly useful in molecular applications. On the contrary, relatively low degree of correlation, expressed by low values of  $K$ , are sufficient to provide reliable and useful-for-chemistry ground-state energy estimates. Although this conclusion may not be correct for *excited-state* calculations, it is likely valid for the singlet-triplet gap calculations that are relevant to designing new phosphorescent materials for the OLED industry.

In perspective, it is interesting to test our developments of a wider class of molecules, especially containing large open-shell subsystems (“molecular magnets”), larger industrially relevant molecules, like phosphorescent and fluorescent transition-metal complexes, transition-metal catalysts [79], and other challenging systems.

### Appendix A: Implementation of $E^{[K]}(\mathbf{t})$

Equation (13) is evaluated in two stages. First, all intermediates that are independent from amplitudes are computed and stored. We call this stage a *compilation* stage. Second, at a *computation* stage energies and gradients from provided amplitudes are evaluated; they can be subsequently used in gradient-based optimisation methods like L-BFGS [62].

The **compilation** stage consists of the following steps:

1. From an ordered list of operators  $(-\mathrm{i}\hat{T}_k)$  [80] that define a QCC Ansatz, generate a list of terms of symmetric polynomials of the orders from 0 to  $K$ . The total number of terms in the expansion is given by Eq. (20).
2. Every term in the list above is a Pauli word  $\hat{T}_{\bar{q}}$  with a unimodular coefficient  $D_{\bar{q}} = \pm 1$  or  $\pm \mathrm{i}$ . We factorize  $\hat{T}_{\bar{q}}$  as in Eq. (15) into a list of phases  $\phi_{\bar{q}}$  and lists of  $\hat{X}_{\bar{q}}$  and  $\hat{Z}_{\bar{q}}$  operators. A list of  $Z_{\bar{q}}$  operators is immediately consumed to evaluate  $f_{\bar{q}}$  [see Eq. (15)], which are merged with the phases  $\phi_{\bar{q}}$  and the corresponding coefficients  $D_{\bar{q}}$ . The resulting phases must be real  $\pm 1$ ; imaginary values signal the error in definition of generators [81] or in the coding.
3. A list of  $\hat{X}_{\bar{q}}$  operators is sorted and unique terms are identified and indexed. A list of lists with positions of the unique  $\hat{X}_q$  operators is created.
4. For the list of unique  $\hat{X}_q$  operators compute and store the Hessian matrix  $\mathbf{H}$  with elements  $\mathbf{H}_{q'q} = \langle 0|\hat{X}_{q'}\hat{H}\hat{X}_q|0\rangle$ . This matrix can also be sparse, so a sparse storage is used to further reduce memory consumption.
5. Normalization factor  $\mathbf{N} = \langle 0|\hat{U}^\dagger(\mathbf{t})\hat{U}(\mathbf{t})|0\rangle$  has unique matrix elements  $\mathbf{N}_{q'q} = \langle 0|\hat{X}_{q'}\hat{X}_q|0\rangle = \delta_{q'q}$

The worst-case complexity of the compilation stage is determined by evaluation of the matrix  $\mathbf{H}$  at the step 4. If the maximum possible order  $K = M$  (the exact energy functional) is selected and all vectors in the expansion of  $\hat{U}(\mathbf{t})|0\rangle$  are linearly independent, one needs to evaluate  $O(4^M)$  matrix elements. For the  $K \ll M$  the length of the expansion is  $O(M^K)$  and one needs  $O(M^{2K})$  matrix elements. The algorithm complexity is, however, linear in the number of terms in the qubit Hamiltonian with a very small prefactor, which allows for either large systems or many iQCC iterations. Terms coalescence (redundancy)

significantly affects the complexity as the size  $\mathbf{H}$  can be much smaller than the length of the expansion (9), but savings are difficult to quantify *a priori* as they are system- and generator list-dependent.

At the **computation** stage trigonometric functions of amplitudes are evaluated first. The remaining steps are:

1. From the list of  $\tan(t_k/2)$  the list of terms of the symmetric polynomials in  $\tan(t_k/2)$  from order  $k = 0$  to  $K$  are generated by the same routine as at the step 1 of the compilation stage. This list is element-wise updated by overall phases computed at the compilation stage and scaled by a product of cosines of amplitudes,  $\prod_{k=1}^K \cos(t_k/2)$ . As a result, a vector  $\mathbf{U}$  representing  $\hat{U}(\mathbf{t})|0\rangle$  for a given set of amplitudes  $\mathbf{t}$  is obtained.
2. The vector  $\mathbf{U}$  from the previous step is multiplied by the Hessian matrix  $\mathbf{H}$  from the left to produce a resulting vector  $\mathbf{HU}$  which is stored separately. In the absence of redundancy this is tantamount to a simple matrix-vector product. Redundancy adds an additional loop structure: one needs to go over all *unique*  $\hat{X}$  terms and for each of them calculate a sum across all occurrence of that term in  $\mathbf{U}$ . To calculate energy, a scalar product of  $\mathbf{U}$  with  $\mathbf{HU}$  is taken and if only energies are requested, explicit storage of  $\mathbf{HU}$  can be avoided. This vector, however, is used in gradient calculations, see Appendix C.

Finally, computed energies and gradients are returned to a caller. Computational complexity of that stage is determined by calculations of the vector  $\mathbf{HU}$ . The computation stage is invoked each time when amplitudes are updated, for example, by iterative optimization.

### Appendix B: Implementation of $F^{[N]}(\mathbf{t})$

Evaluation of  $F^{[N]}(\mathbf{t})$  is done as follows. We iterate by integer  $k$  from 0 to  $(M - 1)$ . Let  $\mathbf{c}_k$  be a real array of coefficients that depend on amplitudes and phases (introduced below), and an array  $\mathbf{w}_k$  which holds the binary representation of the basis product states. The basis-state array  $\mathbf{w}_k$  is stored *sorted* according to the natural binary order of elements; ordering of coefficients is always adjusted accordingly.

Iterations are initialized by setting  $\mathbf{c}_0 = 1$  and  $\mathbf{w}_0 = \text{binary rep } |0\rangle$ .

At the expansion step we perform the following operations:

1. Create a new vector of coefficients  $\tilde{\mathbf{c}}_{k+1} = \sin(t_{M-k})\mathbf{c}_k$ .
  2. Update the current  $\mathbf{c}_k$  by  $\cos(t_{M-k})$ .
  3. Factorize the current operator  $-\mathrm{i}\hat{T}_{M-k}$  into a phase  $\phi_{M-k}$  and operators  $\hat{X}_{M-k}$  and  $\hat{Z}_{M-k}$  that satisfy
- $$-\mathrm{i}\hat{T}_{M-k} = \phi_{M-k}\hat{X}_{M-k}\hat{Z}_{M-k} \quad (\text{B1})$$

Note that for the properly chosen generators  $\hat{T}_k$  the phases  $\phi_k$  come out real ( $\pm 1$ ). The phase  $\phi_{M-k}$  is used to update  $\tilde{\mathbf{c}}_{k+1}$ :

$$\tilde{\mathbf{c}}_{k+1} = \phi_{M-k} \tilde{\mathbf{c}}_{k+1} \quad (\text{B2})$$

4. Evaluate a phase vector  $\mathbf{f}_{M-k}$  by action of the operator  $\hat{Z}_{M-k}$  onto the current basis states vector  $\mathbf{w}_k$ :

$$\hat{Z}_{M-k} \mathbf{w}_k = \mathbf{f}_{M-k} \mathbf{w}_k. \quad (\text{B3})$$

Note that one can avoid explicit storage of  $\mathbf{f}_{M-k}$  because the resulting phases  $\pm 1$  can be immediately combined (merged) with elements of  $\tilde{\mathbf{c}}_{k+1}$ .

5. Create a new basis state vector  $\tilde{\mathbf{w}}_{k+1}$  by action of  $\hat{X}_{M-k}$  on  $\mathbf{w}_k$ :

$$\tilde{\mathbf{w}}_{k+1} = \hat{X}_{M-k} \mathbf{w}_k. \quad (\text{B4})$$

Note that elements of  $\tilde{\mathbf{w}}_{k+1}$  representing the qubit product states are no longer sorted but unique. We sort  $\tilde{\mathbf{w}}_{k+1}$  according to the same ordering as for  $\mathbf{w}_k$ . We also reorder elements of  $\tilde{\mathbf{c}}_{k+1}$  to match the (new) order of elements in the sorted  $\tilde{\mathbf{w}}_{k+1}$ .

6. Now we can *merge* two sorted basis set vectors,  $\mathbf{w}_k$  and  $\tilde{\mathbf{w}}_{k+1}$  into the final  $\mathbf{w}_{k+1}$ . During this process, which is similar to the merge stage of the merge sort algorithm, we can identify the identical elements in both  $\mathbf{w}_k$  and  $\tilde{\mathbf{w}}_k$  and sum up the corresponding coefficients. As a result, the final  $\mathbf{c}_{k+1}$  is produced.

The expansion stage is done. If the length of  $\mathbf{w}_{k+1}$  is less or equal to  $N$  we can continue with the next iteration. Otherwise, we proceed with the *compression (truncation)* stage.

At the compression stage one needs to find a permutation  $p$  the sorts  $\mathbf{c}_{k+1}$  in descending order of absolute values. Then we compute a norm of a “residual” vector  $\mathbf{c}_{k+1}[p[N+1 : \text{end}]]$  (we use the JULIA [60] notation for indexing vectors) to evaluate a re-normalization coefficient  $\lambda_k$ .

Afterwards, we truncate the arrays  $\mathbf{w}_{k+1}$  and  $\mathbf{c}_{k+1}$  to  $N$  via permutation  $p$  as

$$\mathbf{w}_{k+1} = \mathbf{w}_{k+1}[p[1 : N]], \quad (\text{B5})$$

$$\mathbf{c}_{k+1} = \mathbf{c}_{k+1}[p[1 : N]]. \quad (\text{B6})$$

Additionally, the new  $\mathbf{c}_{k+1}$  is multiplied by  $\lambda_k^{-1}$  to restore normalization. The  $k$ -th iteration is complete and one can proceed until  $k = M$ .

Finally, one has to compute the matrix elements  $\langle w_{j'} | \hat{H} | w_j \rangle$ ,  $1 \leq j', j \leq N$  to generate a Hessian matrix

$\mathbf{H}$  (see Sec. II A where  $\hat{X}_q |0\rangle$  play a role of  $|w_j\rangle$ ). The energy  $F^{[N]}(\mathbf{t})$  is computed as a matrix-vector product

$$F(\mathbf{t}) = \mathbf{c}_M^\dagger \mathbf{H} \mathbf{c}_M. \quad (\text{B7})$$

Note that it is not necessary to store the entire matrix  $\mathbf{H}$  explicitly. Instead, one can generate a single row  $\mathbf{H}_{j*}$  and multiply it by  $\mathbf{c}_M$  to generate an element  $(\mathbf{H} \mathbf{c}_M)_j$ . These calculations can be done in parallel on multiple workers assigned to different CPU cores on a shared-memory machine or different processes on distributed-memory architectures, so that the process is expected to be scalable to any numbers of available workers.

### Appendix C: Computing gradients

We commence from the definition of QCC energy, Eq. (3). The partial derivative of it with respect to  $t_k$  amplitude is

$$\frac{\partial E}{\partial t_k} = \left\langle 0 \left| \frac{\partial \hat{U}^\dagger(\mathbf{t})}{\partial t_k} \hat{H} \hat{U}(\mathbf{t}) \right| 0 \right\rangle + \text{c.c} \quad (\text{C1})$$

where c.c stands for complex conjugation. If  $\hat{U}(\mathbf{t})$  is real, which is the case, two terms are equal and we can use the first one as our next step.

Equation (C1) can be interpreted as a scalar product of vectors  $\mathbf{dU}_k = \frac{\partial \hat{U}(\mathbf{t})}{\partial t_k} |0\rangle$  with the vector  $\mathbf{HU}$  (see Sec. II A) which is readily available during energy evaluation.

From the definition of the QCC Ansatz as

$$\hat{U}(\mathbf{t}) = \prod_{k=1}^M \left( \cos(t_k/2) - i \sin(t_k/2) \hat{T}_k \right) \quad (\text{C2})$$

it is clear that taking partial derivative of the expression (C2) with respect to  $t_k$  amounts to replacing the corresponding cos/sin functions in parentheses with their derivatives, namely,  $1/2 (-\sin(t_k/2) - i \cos(t_k/2) \hat{T}_k)$ . That is, at the computation stage one needs to appropriately modify a list of trigonometric functions and the rest of algorithm runs unimpeded to yield a vector  $\mathbf{dU}_k$ . There is one new vector per every gradient component, so  $M$  additional vectors are generated. These vectors are scalar-multiplied to  $\mathbf{HU}$  giving an  $M$ -component gradient vector. A computational overhead of evaluating of a gradient vector is small compared to evaluation of  $\mathbf{HU}$  itself, which is required by energy calculations anyway. Thus, the suggested algorithm is computationally more efficient than other methods of evaluating gradients, such as the parameter-shift rule [28, 30, 82]—in this case the gradient complexity is strictly linear in  $M$ .

---

[1] R. P. Feynman, Int. J. Theor. Phys. **21**, 467 (1982).

[2] S. Lloyd, Science **273**, 1073 (1996).

- [3] T. D. Ladd, F. Jelezko, R. Laflamme, Y. Nakamura, C. Monroe, and J. L. O'Brien, *Nature* **464**, 45 (2010).
- [4] T. Helgaker, P. Jorgensen, and J. Olsen, *Molecular Electronic-structure Theory* (Wiley, 2000).
- [5] N. Marzari, A. Ferretti, and C. Wolverton, *Nat. Mater.* **20**, 736 (2021).
- [6] A. Y. Kitaev, arXiv:quant-ph/9511026 (1995), quant-ph/9511026.
- [7] R. Cleve, A. Ekert, C. Macchiavello, and M. Mosca, *Proc. R. Soc. Lond. A.* **454**, 339 (1998).
- [8] D. S. Abrams and S. Lloyd, *Phys. Rev. Lett.* **83**, 5162 (1999).
- [9] A. Aspuru-Guzik, A. D. Dutoi, P. J. Love, and M. Head-Gordon, *Science* **309**, 1704 (2005).
- [10] B. P. Lanyon, J. D. Whitfield, G. G. Gillett, M. E. Goggin, M. P. Almeida, I. Kassal, J. D. Biamonte, M. Mohseni, B. J. Powell, M. Barbieri, A. Aspuru-Guzik, and A. G. White, *Nat. Chem.* **2**, 106 (2010).
- [11] J. D. Whitfield, J. Biamonte, and A. Aspuru-Guzik, *Mol. Phys.* **109**, 735 (2011).
- [12] P. J. J. O'Malley, R. Babbush, I. D. Kivlichan, J. Romero, J. R. McClean, R. Barends, J. Kelly, P. Roushan, A. Tranter, N. Ding, B. Campbell, Y. Chen, Z. Chen, B. Chiaro, A. Dunsworth, A. G. Fowler, E. Jeffrey, E. Lucero, A. Megrant, J. Y. Mutus, M. Neeley, C. Neill, C. Quintana, D. Sank, A. Vainsencher, J. Wenner, T. C. White, P. V. Coveney, P. J. Love, H. Neven, A. Aspuru-Guzik, and J. M. Martinis, *Phys. Rev. X* **6**, 031007 (2016).
- [13] M. Reiher, N. Wiebe, K. M. Svore, D. Wecker, and M. Troyer, *Proc. Natl. Acad. Sci. USA* **114**, 7555 (2017).
- [14] A. Peruzzo, J. McClean, P. Shadbolt, M.-H. Yung, X.-Q. Zhou, P. J. Love, A. Aspuru-Guzik, and J. L. O'Brien, *Nat. Commun.* **5**, 4213 (2014).
- [15] J. R. McClean, J. Romero, R. Babbush, and A. Aspuru-Guzik, *New J. Phys.* **18**, 023023 (2016).
- [16] A. Kandala, A. Mezzacapo, K. Temme, M. Takita, M. Brink, J. M. Chow, and J. M. Gambetta, *Nature* **549**, 242 (2017).
- [17] J. Lee, W. J. Huggins, M. Head-Gordon, and K. B. Whaley, *J. Chem. Theory Comput.* **15**, 311 (2019).
- [18] J. Romero, R. Babbush, J. R. McClean, C. Hempel, P. J. Love, and A. Aspuru-Guzik, *Quantum Sci. Technol.* **4**, 014008 (2018).
- [19] J. Tilly, H. Chen, S. Cao, D. Picozzi, K. Setia, Y. Li, E. Grant, L. Wossnig, I. Rungger, G. H. Booth, and J. Tenlyson, *Phys. Rep.* **986**, 1 (2022), arXiv:2111.05176v2.
- [20] A. Tranter, P. J. Love, F. Mintert, and P. V. Coveney, *J. Chem. Theory Comput.* **14**, 5617 (2018).
- [21] Z. Jiang, A. Kalev, W. Mruczkiewicz, and H. Neven, *Quantum* **4**, 276 (2020).
- [22] E. Knill, G. Ortiz, and R. D. Somma, *Phys. Rev. A* **75**, 012328 (2007).
- [23] J. Chen, H. Dawkins, Z. Ji, N. Johnston, D. Kribs, F. Shultz, and B. Zeng, *Phys. Rev. A* **88**, 012109 (2013).
- [24] V. Verteletskyi, T.-C. Yen, and A. F. Izmaylov, *J. Chem. Phys.* **152**, 124114 (2020).
- [25] T.-C. Yen, V. Verteletskyi, and A. F. Izmaylov, *J. Chem. Theory Comput.* **16**, 2400 (2020).
- [26] A. F. Izmaylov, T.-C. Yen, R. A. Lang, and V. Verteletskyi, *J. Chem. Theory Comput.* **16**, 190 (2020), arXiv:1907.09040 [quant-ph].
- [27] W. J. Huggins, J. R. McClean, N. C. Rubin, Z. Jiang, N. Wiebe, K. B. Whaley, and R. Babbush, *npj Quantum Inf.* **7**, 23 (2021), arXiv:1907.13117 [quant-ph].
- [28] M. Schuld, V. Bergholm, C. Gogolin, J. Izaac, and N. Killoran, *Phys. Rev. A* **99**, 032331 (2019).
- [29] J. S. Kottmann, A. Anand, and A. Aspuru-Guzik, *Chem. Sci.* **12**, 3497 (2021).
- [30] A. F. Izmaylov, R. A. Lang, and T.-C. Yen, *Phys. Rev. A* **104**, 062443 (2021).
- [31] D. Wecker, M. B. Hastings, and M. Troyer, *Phys. Rev. A* **92**, 042303 (2015).
- [32] I. G. Ryabinkin, T.-C. Yen, S. N. Genin, and A. F. Izmaylov, *J. Chem. Theory Comput.* **14**, 6317 (2018), arXiv:1809.03827 [quant-ph].
- [33] H. R. Grimsley, S. E. Economou, E. Barnes, and N. J. Mayhall, *Nat. Commun.* **10**, 3007 (2019), arXiv:1812.11173 [quant-ph].
- [34] R. A. Lang, I. G. Ryabinkin, and A. F. Izmaylov, arXiv e-prints , arXiv:2002.05701 (2020), arXiv:2002.05701 [quant-ph].
- [35] Y. S. Yordanov, V. Armaos, C. H. W. Barnes, and D. R. M. Arvidsson-Shukur, *Commun. Phys.* **4**, 228 (2021).
- [36] J. K. Freericks, *Symmetry* **14**, 494 (2022).
- [37] I. G. Ryabinkin, R. A. Lang, S. N. Genin, and A. F. Izmaylov, *J. Chem. Theory Comput.* **16**, 1055 (2020).
- [38] F. A. Evangelista, G. K.-L. Chan, and G. E. Scuseria, *J. Chem. Phys.* **151**, 244112 (2019).
- [39] J. Chen, H.-P. Cheng, and J. K. Freericks, *J. Chem. Theory Comput.* **17**, 841 (2021).
- [40] L. Xu and J. K. Freericks, *Symmetry* **15**, 1429 (2023).
- [41] D. Halder, V. S. Prasanna, and R. Maitra, *J. Chem. Phys.* **157**, 174117 (2022).
- [42] S. Tribedi, A. Chakraborty, and R. Maitra, *J. Chem. Theory Comput.* **16**, 6317 (2020).
- [43] R. A. Lang, I. G. Ryabinkin, and A. F. Izmaylov, *J. Chem. Theory Comput.* **17**, 66 (2021), arXiv:2002.05701 [quant-ph].
- [44] A. Endo, K. Suzuki, T. Yoshihara, S. Tobita, M. Yahiro, and C. Adachi, *Chem. Phys. Lett.* **460**, 155 (2008).
- [45] S. N. Genin, I. G. Ryabinkin, N. R. Paisley, S. O. Whelan, M. G. Helander, and Z. M. Hudson, *Angew. Chem. Int. Ed.* **61**, e202116175 (2022).
- [46] D. S. Steiger, T. Häner, S. N. Genin, and H. G. Katzgraber, arXiv (2024), arXiv:2404.10047 [quant-ph].
- [47] Eq. (9) is, in fact, a *generating function*.
- [48] I. Macdonald, *Symmetric Functions and Hall Polynomials*, Oxford classic texts in the physical sciences (Clarendon Press, 1998).
- [49] S. R. White, *Phys. Rev. Lett.* **69**, 2863 (1992).
- [50] U. Schollwöck, *Ann. Phys.* **326**, 96 (2011).
- [51] R. Orús, *Ann. Phys.* **349**, 117 (2014).
- [52] B. Cooper and P. J. Knowles, *J. Chem. Phys.* **133**, 234102 (2010).
- [53] We use lowercase bold letters to denote vectors in  $2^n$  qubit Hilbert space and capital bold letters to define subspaces where those vectors live in.
- [54] L. Brillouin, *J. Phys. Radium* **3**, 373 (1932).
- [55] E. P. Wigner, in *Part I: Physical Chemistry. Part II: Solid State Physics* (Springer Berlin Heidelberg, 1997) pp. 131–136.
- [56] I. G. Ryabinkin, A. F. Izmaylov, and S. N. Genin, *Quantum Sci. Technol.* **6**, 024012 (2021).
- [57] M. W. Schmidt, K. K. Baldridge, J. A. Boatz, S. T. Elbert, M. S. Gordon, J. H. Jensen, S. Koseki, N. Matsunaga, K. A. Nguyen, S. J. Su, T. L. Windus, M. Dupuis, and J. Montgomery, *J. Comput. Chem.* **14**, 1347 (1993).
- [58] M. S. Gordon and M. W. Schmidt, in *Theory and Appli-*

- cations of Computational Chemistry. The first forty years*, edited by C. E. Dykstra, G. Frenking, K. S. Kim, and G. E. Scuseria (Elsevier, Amsterdam, 2005) pp. 1167–1189.
- [59] R. M. Parrish, L. A. Burns, D. G. A. Smith, A. C. Simmonett, A. E. DePrince, 3rd, E. G. Hohenstein, U. Bozkaya, A. Y. Sokolov, R. Di Remigio, R. M. Richard, J. F. Gonthier, A. M. James, H. R. McAlexander, A. Kumar, M. Saitow, X. Wang, B. P. Pritchard, P. Verma, H. F. Schaefer, 3rd, K. Patkowski, R. A. King, E. F. Valeev, F. A. Evangelista, J. M. Turney, T. D. Crawford, and C. D. Sherrill, *J. Chem. Theory Comput.* **13**, 3185 (2017).
  - [60] J. Bezanson, A. Edelman, S. Karpinski, and V. B. Shah, *SIAM Review* **59**, 65 (2017).
  - [61] R. Byrd, P. Lu, J. Nocedal, and C. Zhu, *SIAM J. Sci. Comput.* **16**, 1190 (1995).
  - [62] C. Zhu, R. H. Byrd, P. Lu, and J. Nocedal, *ACM Trans. Math. Softw.* **23**, 550 (1997).
  - [63] S. G. Johnson, *The nlopt nonlinear-optimization package*, online (2020), julia package at <https://github.com/JuliaOpt/NLopt.jl>.
  - [64] P. S. Epstein, *Phys. Rev.* **28**, 695 (1926).
  - [65] R. Nesbet, *P. Roy. Soc. A - Math. Phys.* **230**, 312 (1955).
  - [66] T. H. Dunning, *J. Chem. Phys.* **90**, 1007 (1989).
  - [67] J. Ivanic and K. Ruedenberg, *Theor. Chem. Acc.* **106**, 339 (2001).
  - [68] I. G. Ryabinkin, S. N. Genin, and A. F. Izmaylov, *J. Chem. Theory Comput.* **15**, 249 (2019), arXiv:1806.00461 [physics.chem-ph].
  - [69] P. Lykos and G. W. Pratt, *Rev. Mod. Phys.* **35**, 496 (1963).
  - [70] S. Bravyi, J. M. Gambetta, A. Mezzacapo, and K. Temme, ArXiv e-prints , 1701.08213 (2017), arXiv:1701.08213 [quant-ph].
  - [71] K. Setia, R. Chen, J. E. Rice, A. Mezzacapo, M. Pistoia, and J. D. Whitfield, *J. Chem. Theory Comput.* **16**, 6091 (2020), arXiv:1910.14644 [quant-ph].
  - [72] H. R. Grimsley, D. Claudino, S. E. Economou, E. Barnes, and N. J. Mayhall, *J. Chem. Theory Comput.* **16**, 1 (2020).
  - [73] A. F. Izmaylov, M. Díaz-Tinoco, and R. A. Lang, *Phys. Chem. Chem. Phys.* **22**, 12980 (2020).
  - [74] M. R. Hirshbrunner, D. Chamaki, J. W. Mullinax, and N. M. Tubman, *Quantum* **8**, 1538 (2024).
  - [75] J. Chen, H.-P. Cheng, and J. K. Freericks, *J. Chem. Theory Comput.* **18**, 2193 (2022).
  - [76] P. C. Hariharan and J. A. Pople, *Theoret. Chim. Acta* **28**, 213 (1973).
  - [77] S. Genin and M. Helander, iQCC Hamiltonians for small molecules, online (2024).
  - [78] W. J. Stevens, M. Krauss, H. Basch, and P. G. Jasien, *Can. J. Chem.* **70**, 612 (1992).
  - [79] V. von Burg, G. H. Low, T. Häner, D. S. Steiger, M. Reiher, M. Roetteler, and M. Troyer, *Phys. Rev. Research* **3**, 033055 (2021).
  - [80] It is convenient to include a factor ( $-i$ ) into the definition of generators.
  - [81] Generators  $\hat{T}_k$  of the QCC unitary must be chosen so as to contain the *odd* number of  $\hat{y}$  Pauli elementary operators to ensure they are *imaginary* (*i.e.* have purely imaginary matrix elements in the computational basis), or, equivalently  $-i\hat{T}_k$  are *real* operators.
  - [82] J. S. Kottmann, A. Anand, and A. Aspuru-Guzik, *Chem. Sci.* **12**, 3497 (2021).